Radiology Case Reports 14 (2019) 1334–1347

Available online at www.sciencedirect.com

ScienceDirect

journal homepage: www.elsevier.com/locate/radcr

Case Report

Glioblastoma with extracranial parotid, lymph node, and pulmonary metastases: a case report

Jeroen Swinnen, MD[a,b,*], *Geert Gelin, MD*[a], *Sabine Fransis, MD*[c], *Jan Vandevenne, MD, PhD*[a,d], *Sofie Van Cauter, MD, PhD*[a,b]

[a] *Department of Radiology, Ziekenhuis Oost-Limburg, Schiepse Bos 6, 3600 Genk, Belgium*
[b] *Department of Radiology, University Hospitals Leuven, Herestraat 49, 3000 Leuven, Belgium*
[c] *Department of Pathology, Ziekenhuis Oost-Limburg, Schiepse Bos 6, 3600 Genk, Belgium*
[d] *Faculty of Medicine, University of Hasselt, Agoralaan gebouw D, 3590 Diepenbeek, Belgium*

ARTICLE INFO

Article history:
Received 26 May 2019
Revised 7 August 2019
Accepted 9 August 2019
Available online 5 September 2019

Keywords:
Glioblastoma
Isocitrate dehydrogenase
Lung
Metastasis
Neoplasm
Parotid gland

ABSTRACT

We present a rare case of an isocitrate dehydrogenase-wildtype glioblastoma with histologically proven parotid, cervical lymph node, and lung metastases. While recent therapy advances are likely to increase glioblastoma mid- and long-term survival, this will also increase the time window for extraneural glioblastoma spread. Radiologists should be aware of this risk, so they can accurately detect and interpret metastatic glioblastoma disease.

Background

Glioblastoma (GBM) is the most common primary malignant brain tumor [1,2]. Nevertheless, extraneural metastases of GBM are uncommon [3–6]. We present a case of a GBM with histologically proven parotid, cervical lymph node, and lung metastases. To the best of our knowledge, only 10 cases of GBM metastases to the parotid gland have been reported [7–16].

Case report

A 56-year-old woman presented to her general practitioner with a 3- to 4-week history of progressive diurnal headaches, nausea, and vomiting. Symptom relief was initially obtained by self-medication with ibuprofen, but the effectiveness diminished gradually. No weight loss, fever, or night sweats were noted. Vital signs were normal on physical examination. Medical history included arterial hypertension and morbid obesity.

Acknowledgment: Special thanks to Ms. Leentje Dreesen for proofreading the manuscript.
Declaration of Competing Interest: The authors have declared that no competing interests exist.

* *Corresponding author.*
E-mail address: Jeroen.swinnen@uzleuven.be (J. Swinnen).

https://doi.org/10.1016/j.radcr.2019.08.011

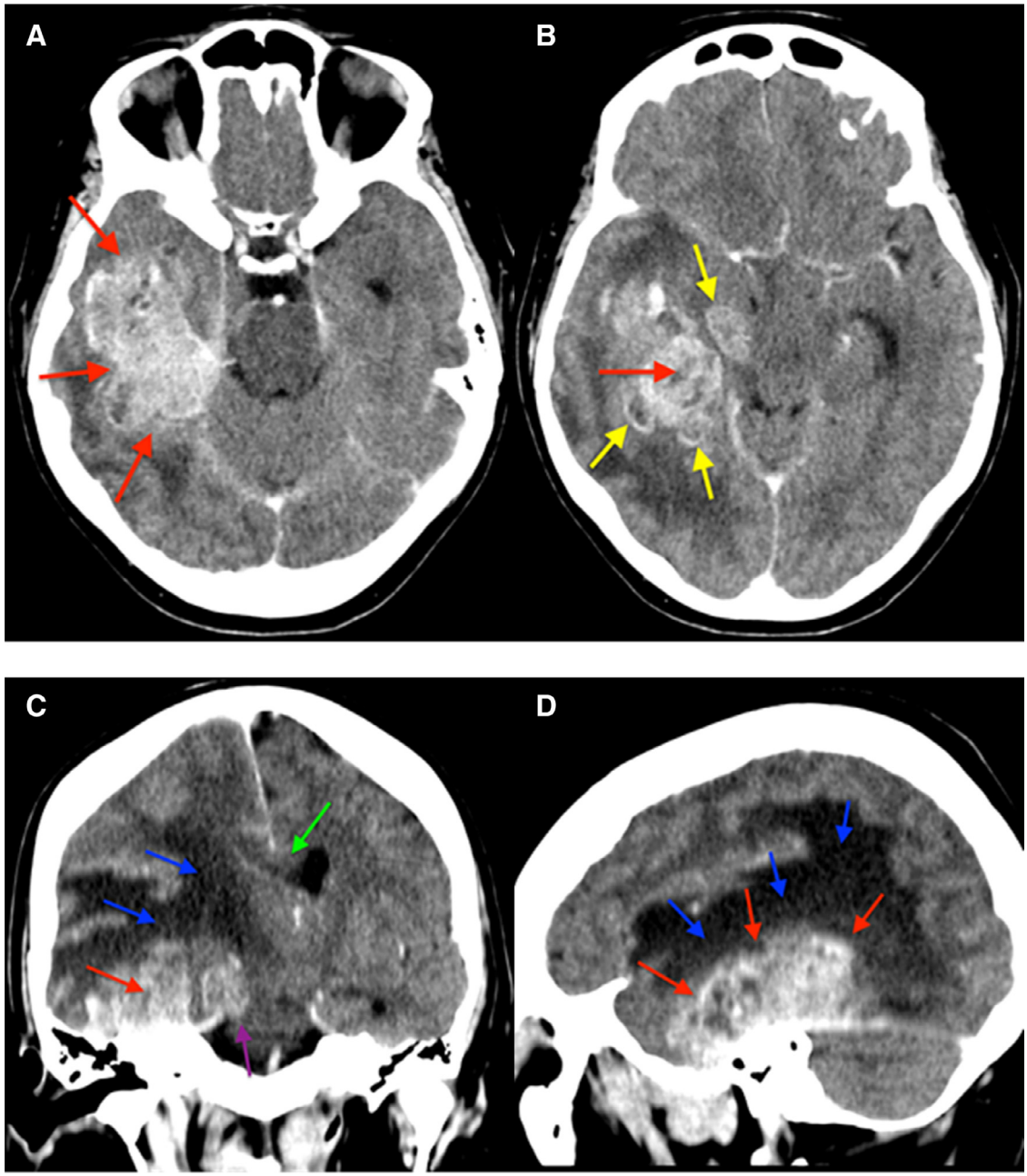

Fig. 1 – (A-D) Iodine contrast-enhanced brain CT performed at an external imaging center showing a contrast-enhancing mass (red arrows) in the right temporal lobe abutting the tentorium cerebelli. Extensive perilesional edema (blue arrows) and secondary uncal (purple arrow) and subfalcine (green arrow) herniation were present. The mass was surrounded by multiple nodular satellite lesions (yellow arrows).

Chronic medication use was limited to oral spironolactone 25 mg once daily.

The patient was referred by her family doctor for a computed tomography (CT) scan of the brain at an external imaging center. Contrast-enhanced CT of the brain showed a mass in the right temporal lobe abutting the tentorium cerebelli (Fig. 1). Extensive perilesional edema and mass effect were present, with secondary right-sided uncal herniation and subfalcine herniation to the left. The temporal mass showed heterogenous contrast uptake, most pronounced in the periphery of the lesion. The mass was also surrounded by multiple nodular contrast-enhancing lesions, suggestive of satellite lesions. Noncontrast CT of the brain could not be obtained from the external imaging center. After receiving the report of the external CT scan, the family doctor referred the patient to our emergency department for complete diagnostic evaluation and treatment. Additional physical and neurologic examination showed a slightly unstable gait, but no other relevant

findings. Neuron-specific enolase tumor marker was slightly elevated at a value of 28.3 μg/L with upper limit 16.3 μg/L. No other relevant laboratory findings were noted. Venous phase CT scan of the chest and abdomen showed no significant abnormalities.

Magnetic resonance imaging (MRI) of the brain 1 day after presentation showed a mass in the right temporal lobe abutting the right tentorium cerebelli (Fig. 2). On T2-FLAIR imaging, the mass was slightly hyperintense compared to the surrounding parenchyma. Extensive perilesional edema was noted in the right temporal lobe, right insula, right lentiform nucleus, and posterior limb of the internal capsule. Multiple hypointense spots were spread throughout the mass on T2* gradient echo imaging, compatible with intralesional hemosiderin or calcific deposits. On B1000 imaging, the mass contained areas of hyperintensity corresponding to areas of iso- to hypointensity on ADC imaging, suggestive of a hypercellularity of the mass. On gadolinium-enhanced T1-weighted images, the temporal mass showed avid contrast enhancement with areas of central sparing. As noted on CT imaging, the mass was surrounded by multiple nodular enhancing satellite lesions. Perfusion-weighted MR or MR spectroscopy imaging was not performed. Our initial differential diagnosis included GBM, metastasis, and hemangiopericytoma with a preference for GBM.

Surgical resection of the mass and its satellite lesions was performed 8 days after presentation. Intraoperative frozen section of a specimen concluded a high-grade malignant tumor. Microscopic examination of the mass showed a cell-rich tumor with a high rate of anisokaryosis as well as necrosis and endothelial proliferation (Fig. 3). Immunohistochemical staining showed diffuse p53 positivity of tumor cells, glial fibrillary acidic protein (GFAP) positivity, and a Ki-67 labeling index of 20%. Following negative IDH-1 staining, tissue was sent for IDH-1 and IDH-2 exon analysis, which were also negative. O6-methylguanin-DNA-methyltransferase methylation status was not performed. Final diagnosis concluded an IDH-wildtype GBM.

MRI of the brain 72 hours after surgery showed subtle nodular contrast-enhanced thickening of the right tentorium cerebelli at the level of the resection cavity, compatible with residual tumor or granulation tissue (Fig. 4). At the level of the right parotid gland or cervical levels, no enhancing lymph nodes were present.

The patient received radiotherapy plus concomitant and adjuvant temozolomide as defined by Stupp protocol [17]. Radiation therapy on the resection area was administered in 30 doses of 2 gray on weekdays. Concomitant oral temozolomide was prescribed at a ratio of 75 mg/m² daily. Furthermore, oral levetiracetam 500 mg 2 times daily was added for seizure prophylaxis. After completion of radiation therapy, the adjuvant temozolomide regimen was changed to 200 mg/m² intake 5 days per week for 4 weeks, repeated in 6 cycles. Oral methylprednisolone 32 mg was continued once daily.

MRI of the brain 3.5 months after presentation showed multiple contrast-enhancing nodules at the medial border of the resection cavity, suggestive of local recurrence (Fig. 5). Perfusion-weighted imaging showed an increased relative cerebral blood volume in the area of recurrence. Furthermore, 3 enhancing nodules were present in the right parotid gland. The 2 largest nodules were hyperintense on B1000 imaging. Nevertheless, these parotid nodules were missed on initial reporting. A repeat MRI scan was planned 5.5 months after presentation. Meanwhile, treatment remained unchanged.

Follow-up MRI of the brain 5.5 months after presentation showed a significant volume increase of the contrast-enhancing nodules medial to the resection cavity, again consistent with local recurrence (Fig. 6). An increased relative cerebral blood flow was noted in the area of recurrence. Furthermore, the parotid nodules were detected on this examination. Retrospectively, the contrast-enhancing nodules in the parotid gland also showed moderate volume increase and a slight increase in B1000 hyperintensity. On anamnesis, the patient admitted pain and swelling at the level of the right parotid gland, which she had not yet reported. Empiric treatment with oral amoxicillin/clavulanic acid 875/125 mg 3 times daily proved not to be effective.

Subsequent CT of the neck 6 months after presentation showed multiple lymph nodes in the right parotid gland and right cervical levels 2, 3, 1B, and 5 (Fig. 7A-C). Furthermore, 3 nodules were observed in the right lung apex, the largest measuring 5 mm in the longest axial diameter (Fig. 7D). These nodules were not present on a venous phase contrast-enhanced CT of the chest and abdomen at initial presentation. A new venous phase contrast-enhanced CT of the chest showed multiple bilateral millimetric solid lung nodules with rounded edges (Fig 7E-F). No enlarged mediastinal, hilar, or axillary lymph nodes were noted. The patient complained of general fatigue but did not suffer from dyspnea on anamnesis. No neurologic motor or sensory deficit was noted at this point.

Ultrasound-guided fine-needle aspiration cytology (FNAC) of a parotid lesion was performed 6.5 months after presentation (Fig. 8A-C). Cells showed hyperchromatic nuclei, with irregular nuclear membranes with prominent nucleoli and nuclear pseudoinclusions. Immunohistochemical staining was negative for Pan-CK, CK-7, CK20, p63, S100, and LCA markers, therefore excluding metastatic or primary carcinoma, melanoma, or lymphoma. Immunohistochemical staining was positive for GFAP. This cytology was compared to the GFAP expressing GBM, which showed similar morphologic and immunohistochemical profiles. Additional p53-staining showed overexpression similar to the GBM. Therefore, a tentative diagnosis of metastatic GBM was made. Because of this unusual presentation, additional tissue confirmation was advised.

Subsequent resection of a cervical lymphadenopathy was performed 7 months after presentation (Fig. 8D-F). Cell morphology was similar to parotid FNAC, with presence of anisokaryosis and nuclear inclusions. Immunohistochemical staining was negative for Pankeratin and EMA epithelial markers. Diffuse overexpression of S100 and GFAP was present. The possibility of S100 positive melanoma metastases was excluded by additional negative staining for MITF, HMB45, and Mart-1.

Thoracoscopic biopsy of a solid lung nodule in the left lower lung lobe was performed 7.5 months after presentation (Fig. 8G-I). Microscopic examination showed nests and strands of spindle-like and epithelioid cells with anisokaryosis. Immunohistochemical staining showed overexpression of GFAP

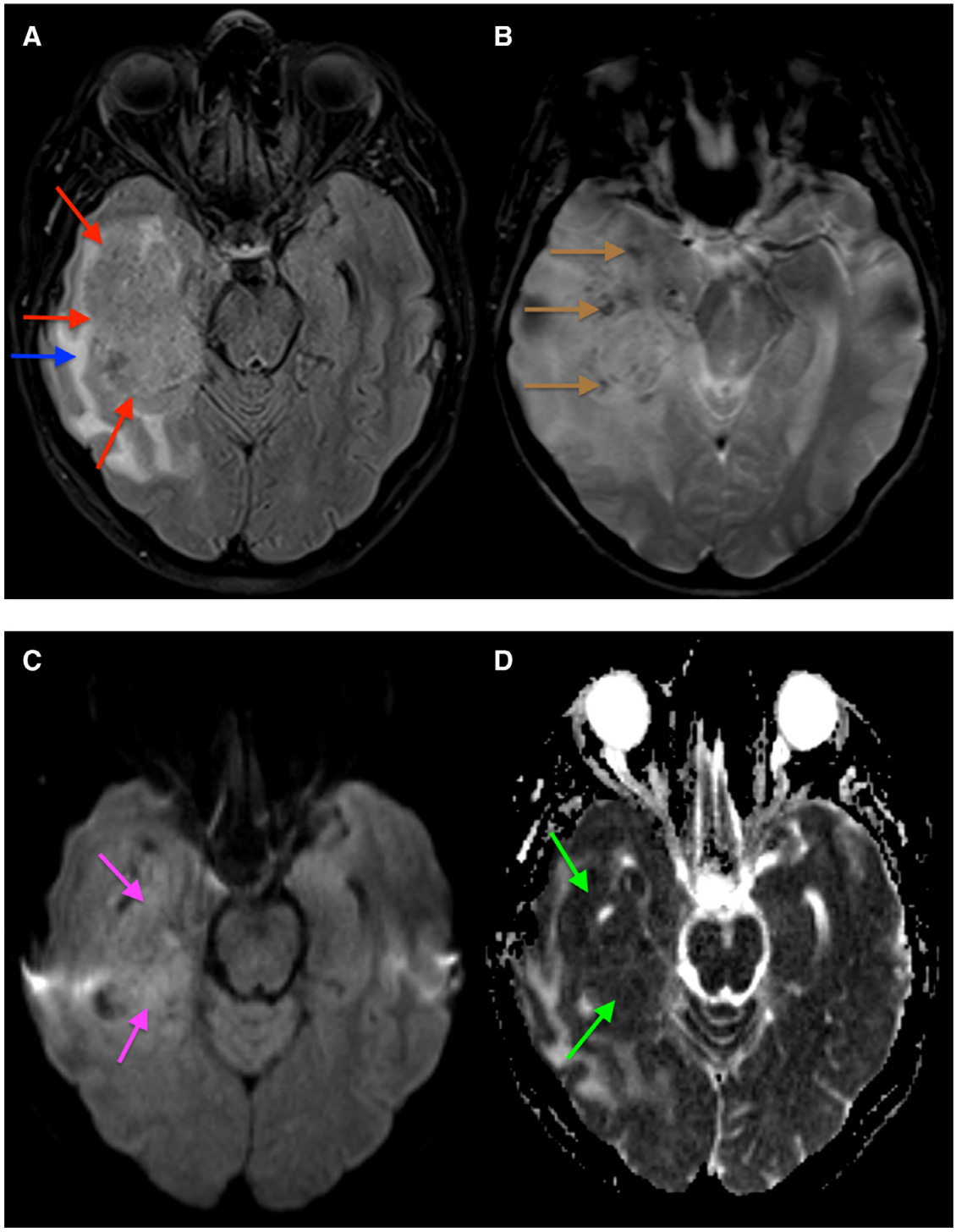

Fig. 2 – MRI of the brain at initial presentation. (A) FLAIR image showing a slightly hyperintense mass (red arrows) compared to the surrounding parenchyma, with extensive perilesional edema (blue arrow). (B) T2* gradient echo image showing multiple hypointense dots (brown arrows) spread throughout the lesion, most likely corresponding hemosiderin or calcifications. (C) B1000 image demonstrating hyperintense areas in the mass (purple arrows). (D) ADC map showing corresponding areas of iso- to hypointensity (green arrows), suggestive of a hypercellular mass. (E) T1-weighted image showing a hypointense mass (orange arrows). (F-J) Gadolinium-enhanced T1-weighted images showing avid contrast enhancement of the temporal mass (blue arrows) with areas of central sparing. The mass was surrounded by multiple nodular satellite lesions (yellow arrows).

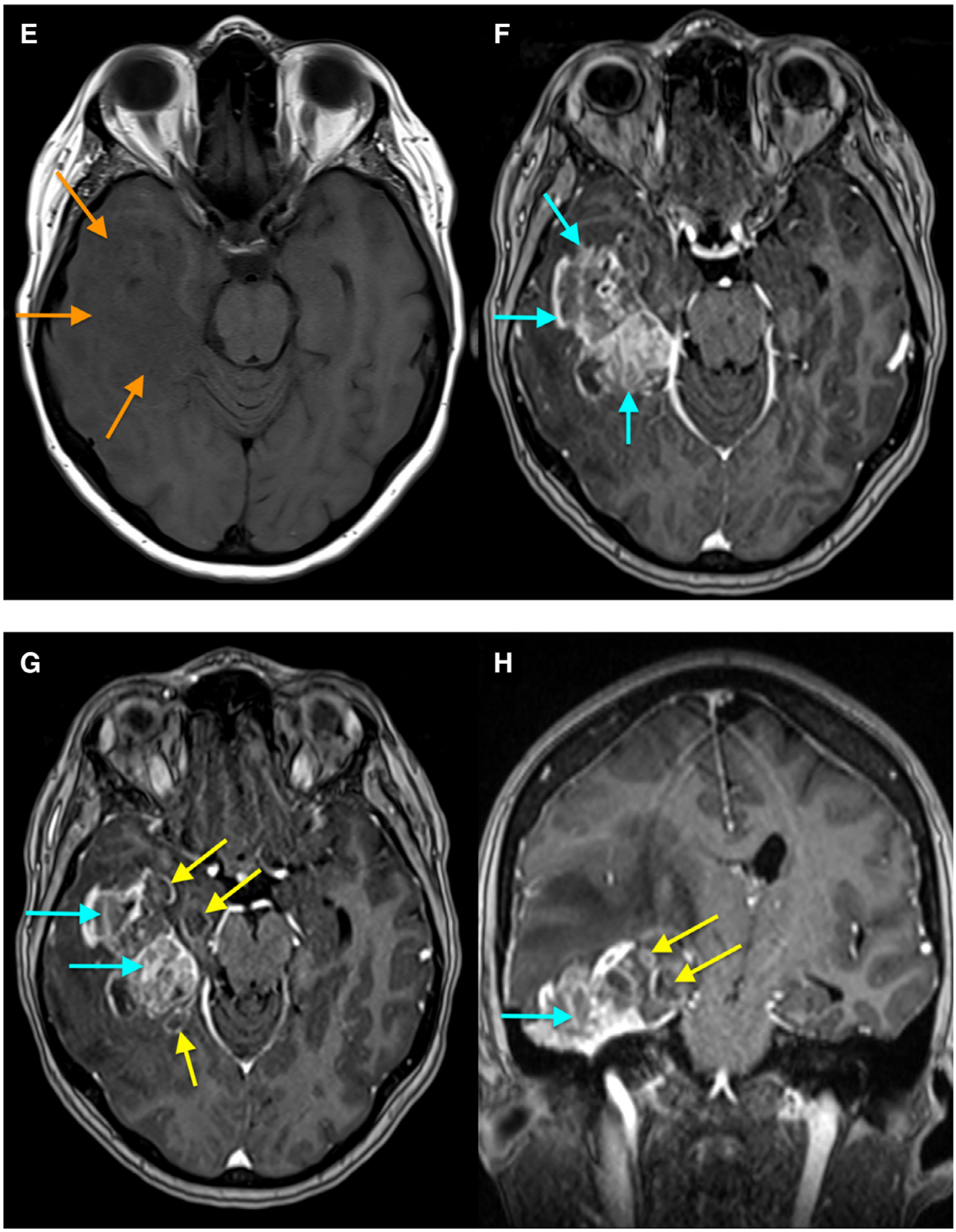

Fig. 2 – Continued

and vimentin, as well as light staining for S-100. Staining was negative for EMA and Pan-CK epithelial markers. These findings were compatible with metastasis of the known GBM.

After obtaining the final diagnosis of metastatic GBM, the patient was referred to another hospital for clinical trial treatment. The patient was started on oral VEGFR 1-3 inhibitor (axitinib) and anti-PD-L1 IgG1 antibody (avelumab) treatment. External medical reports noted intracranial disease stability on a follow-up MRI scan 10 months after presentation. Follow-up MRI of the brain 11 months after presentation concluded new areas of intracranial contrast enhancement in the right anterior temporal lobe, right parietal lobe, and right centrum semiovale. These external images could not be obtained. At the same time, the patient developed a malignant pleuritis for which a pleurodesis was performed at the external hospital. During recovery, the patient developed a rapidly progressive

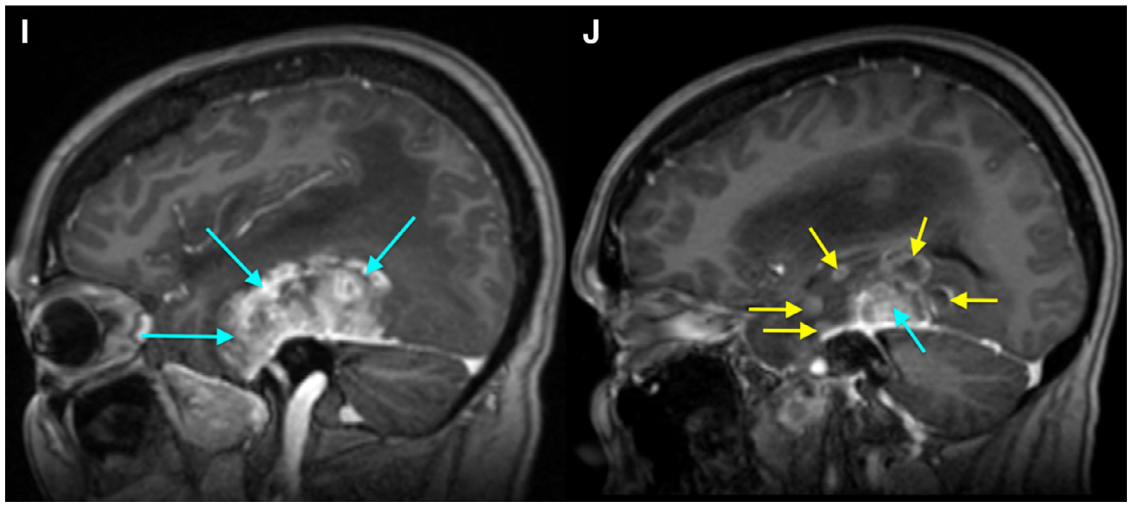

Fig. 2 – Continued

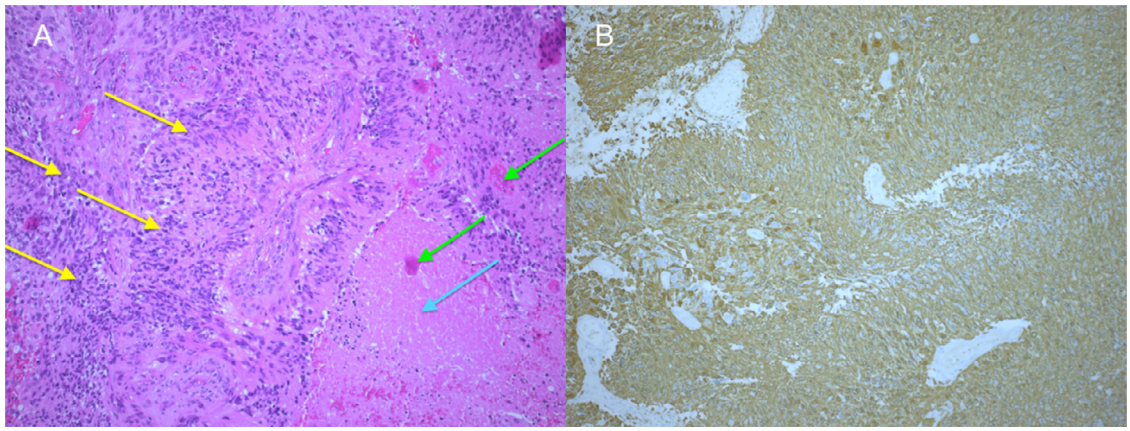

Fig. 3 – Resection specimen of brain tissue and glioblastoma (GBM) (10×). (A) H&E stain showing GBM with palisaded highly atypical cells (yellow arrows) next to geographic necrosis (blue arrow) and high endothelial venules (green arrows). (B) Tumoral cells are diffusely GFAP positive (brown staining), indicating glial origin.

left-sided hemiparesis, for which a follow-up MRI of the brain was performed 12.5 months after presentation (Fig. 9). This MRI showed cystic encephalomalacia of the resection cavity with surrounding local recurrence. Furthermore, an intracranial contrast-enhancing metastasis was present in the right superior frontal gyrus and body of the corpus callosum, with a corresponding area of increased rCBF. FLAIR imaging revealed significant perilesional edema extending to the precentral and to a lesser extent to the postcentral gyrus.

Clinical trial treatment was stopped, and the patient was started on lomustine monotherapy, 160 mg orally once every 6 weeks. Unfortunately, the patient died 14.5 months after presentation.

Discussion

GBM is the most common glioma histology, comprising 56% of gliomas [1]. GBM accounts for 14.7% of all primary CNS tumors and 47.7% of primary malignant CNS tumors [1]. Diagnosis of GBM is associated with a very poor outcome, as estimated 5-year survival is 5.6% [1]. Since the 2016 WHO revision, GBM is divided into IDH-wildtype, IDH-mutant, and "not otherwise specified" (NOS) subgroups [2]. For IDH-wildtype GBM, which account for almost 90% of GBM, the median age at diagnosis is 62 years and median survival after Stupp protocol is 15 months [2]. For IDH-mutant GBM, which account for the remaining 10%, the median age at diagnosis is 44 years and median survival after Stupp protocol is 31 months [2].

Estimated incidence of extra-CNS GBM metastases ranges 0.2%-2.0% [4–6]. Median age at diagnosis ranges 38-42 years, which is younger than the median age for IDH-wildtype diagnosis but similar to IDH-mutant [2,4,5]. Extracranial metastases seem to be more prevalent in men than women, with a male-to-female ratio of 2-3 to 1 [3,4]. The occurrence of extraneural metastasis significantly shortens GBM survival, with a subsequent median overall survival of 1.5-6.0 months [5].

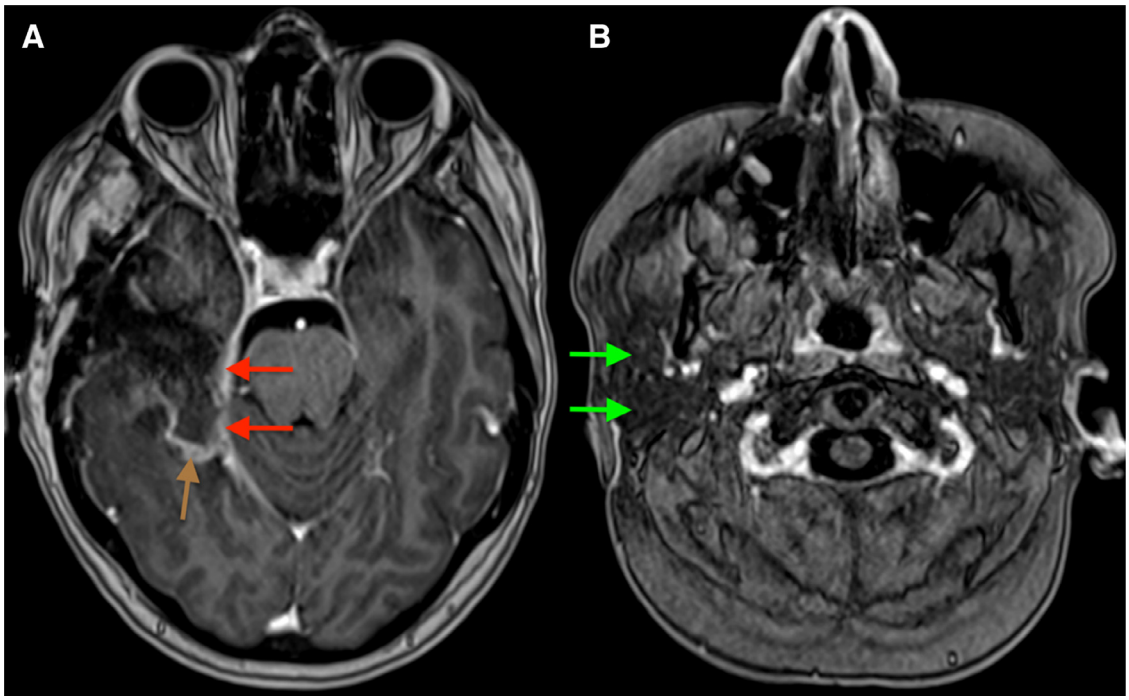

Fig. 4 – Gadolinium-enhanced T1-weighted imaging 72 hours after resection. (A) At the level of the resection cavity, subtle nodular thickening of the right tentorium cerebelli was noted (red arrows), compatible with granulation tissue or residual tumor. Residual blood products were also present (brown arrow). (B) At the level of the right parotid gland (green arrows), no enhancing lymph nodes were present.

Primary site of metastases seems to influence prognosis, with lung metastasis being the most negative predictor, resulting in a survival loss of 2.7 months [5].

Metastatic disease can occur through hematogenous, lymphogenous, or cerebrospinal fluid spread. Dissemination via a ventricular shunt has also been reported [4]. During embryologic development, lymph nodes and lymphogenous tissue are incorporated within the parotid gland. In general, metastases to the parotid gland develop most frequently by lymphogenous spread and rarely by hematogenous spread or continuous growth [18]. In our case, a hematogenous or mixed spread pattern can certainly not be excluded, as our patient also developed lung metastases.

Several theories exist why GBM does not have the tendency to metastasize, referring to several morphologic and histologic characteristics of the brain, such as the absence of a true lymphatic system or connective stroma in the cerebrum, the constituency of the blood-brain barrier and dural membranes, as well as immunologic features of glioma cells [4]. Furthermore, the median short survival is likely to prevent the development and detection of metastatic disease [3–5].

Introduction of advanced therapies such as proton-, immune-, and gene therapy will likely increase long-term survival of GBM patients [19]. As more patients also become eligible for surgery or radiation therapy, iatrogenic disruption of the blood-brain barrier becomes standard [4]. This provides more time and more pathways for the GBM to metastasize. Furthermore, the recent discovery of peripherally circulating tumor cells (CTCs) in GBM patients challenges the assumption that GBM does not disseminate [20]. Prolonged survival may therefore correspond to an increased risk for metastases. As the median survival is the longest for the IDH-mutant GBM, this subtype might be more prone to metastasize than the IDH-wildtype subtype [2]. However, this was not the case in our patient, who presented with an IDH-wildtype GBM.

Although reports of GBM metastases have increased over time, it is important to note that this remains a rare diagnosis [3]. For all patients with a concomitant intracranial GBM and metastatic disease pattern, a second primary malignancy is much more likely and should always be excluded first. Prior to the biopsy of metastatic locations, our differential diagnosis included a synchronous metastatic malignancy, GBM metastases, multifocal lymphoproliferative disease as well as an autoinflammatory disease process. In our case, initial suspicion of metastatic GBM was put forward by the radiologist who detected the ipsilateral parotid nodules. This suspicion was confirmed by the pathologist on interpretation of the parotid FNAC. A definite diagnosis, however, could only be made by a thorough pathologic comparison of the primary GBM with biopsies from different metastatic locations. As cell morphology and immunohistochemistry were so consistent across all pathologic specimens, the final diagnosis could be made with confidence.

The occurrence of extra-CNS metastasis from GBM shortens the overall survival significantly compared to typical in-

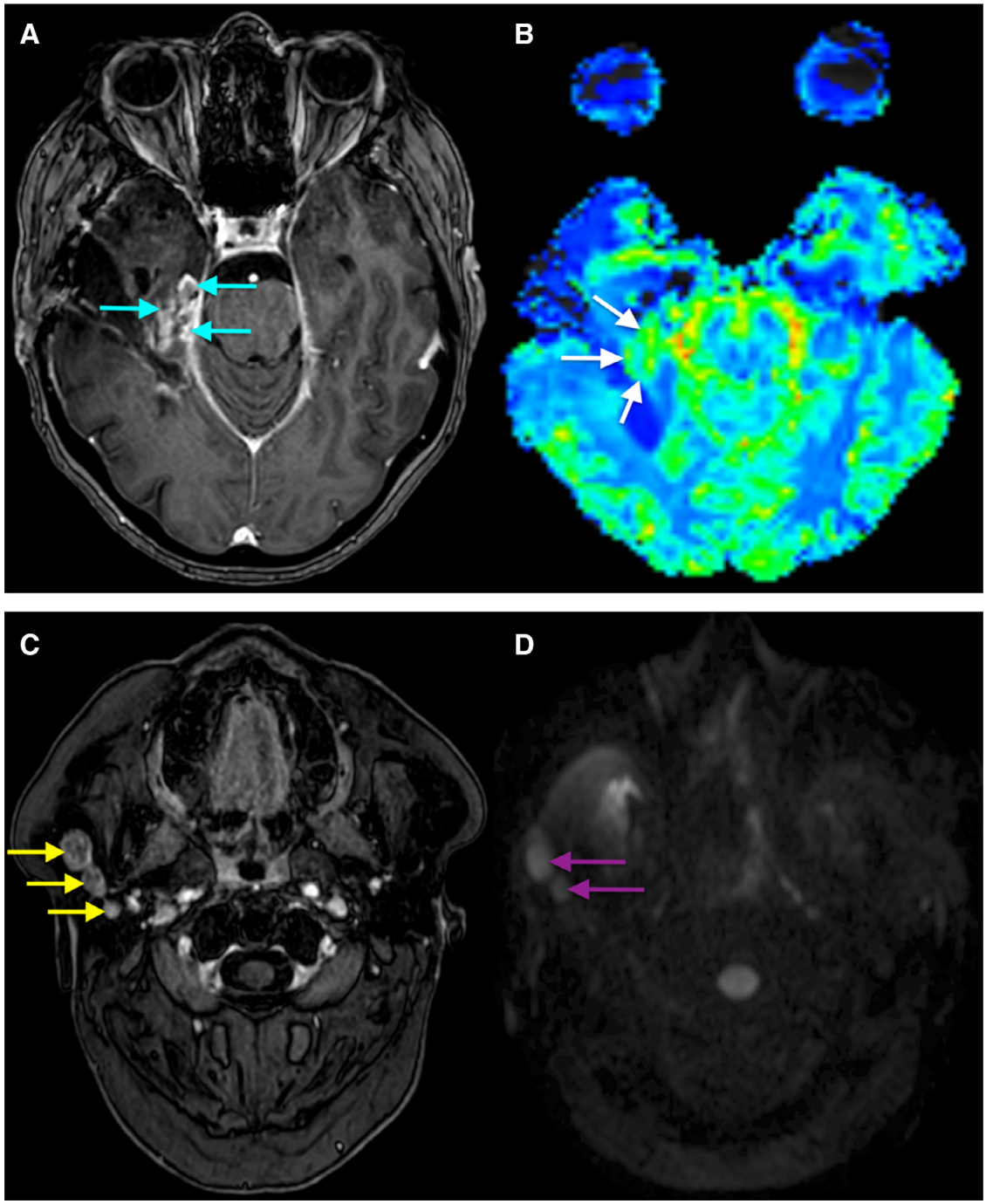

Fig. 5 – MRI of the brain 3.5 months after presentation. (A) Gadolinium-enhanced T1-weighted image showing nodular recurrence (blue arrows) medial to the resection cavity. (B) Perfusion-weighted imaging showing an increased relative cerebral blood volume (white arrows) in the area of recurrence. (C) Gadolinium-enhanced T1-weighted image showing 3 enhancing nodules (yellow arrows) in the right parotid gland, suggestive of lymphadenopathy. (D) B1000 image demonstrating hyperintensity of the 2 largest parotid nodules (purple arrows). Nevertheless, the parotid nodules were missed on the initial report.

tracranial GBMs [5]. In our patient, all 3 extraneural metastatic locations caused symptoms and deterioration of the patient. Parotid and cervical lymph node metastases caused pain and swelling. Lung metastases presumptively caused a malignant pleuritis requiring pleurodesis. However, most morbidity was probably caused by an intracranial metastasis in the area of the right corticospinal tract and motor cortex, leading to a rapidly progressive left-sided hemiparesis. Piccirilli et al.

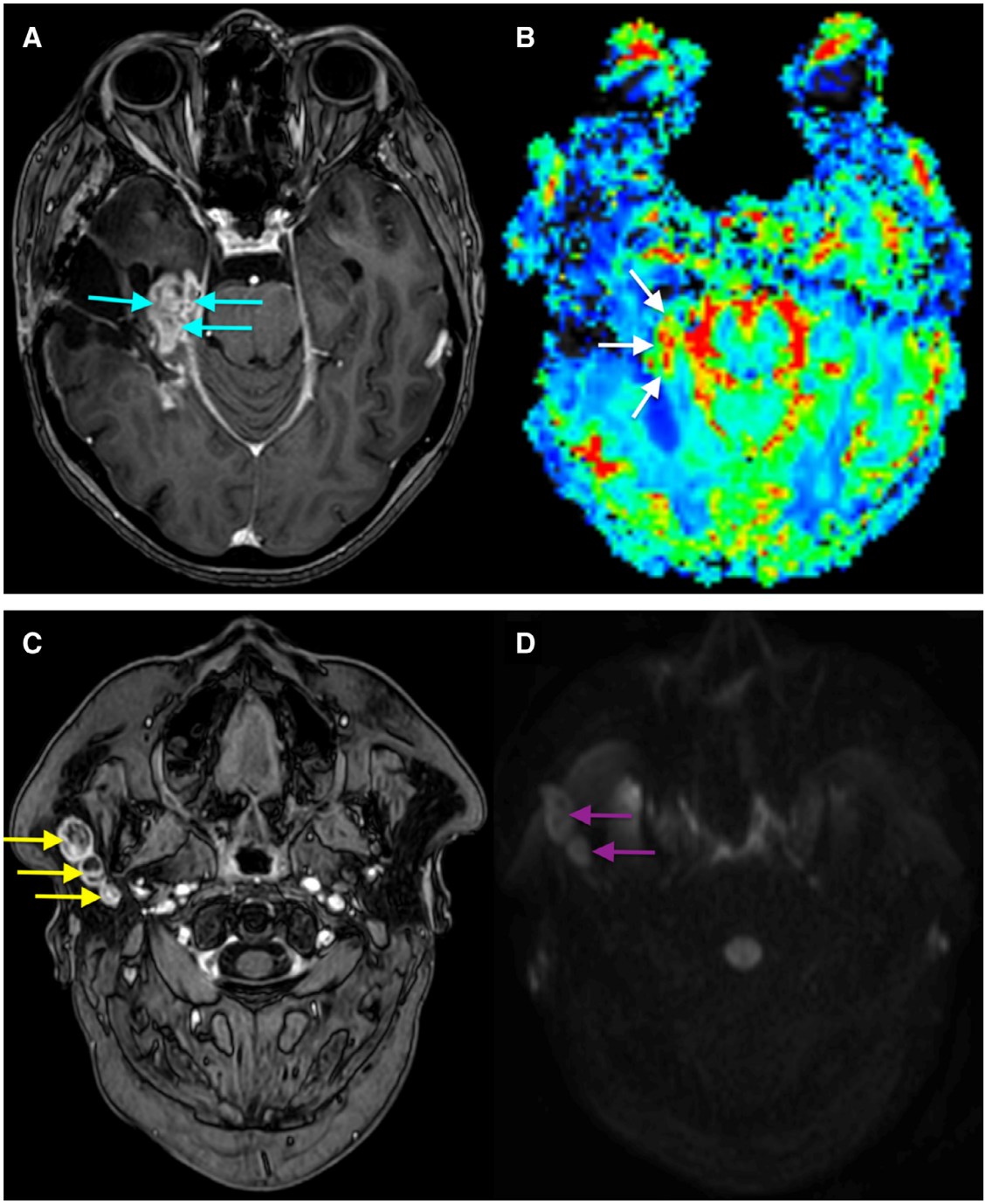

Fig. 6 – MRI of the brain 5.5 months after presentation. (A) Gadolinium-enhanced T1-weighted image showing a volume increase of local recurrence. (B) Perfusion-weighted imaging demonstrating an increased relative cerebral blood flow (rCBF) in the area of recurrence. (C) Gadolinium-enhanced T1-weighted image showing a moderate volume increase of the parotid nodules. (D) On B1000 imaging, the parotid nodules had also grown in volume. On this examination, the parotid nodules were detected.

noted that in their case series, each death was the result of cerebral GBM regrowth rather than metastases [4]. This was probably not the case in our patient, as the clinical effect of intracranial and lung metastases was so predominant.

No standard treatment protocol is currently available for extracranial GBM metastases. Nevertheless, Lun et al. observed a trend for increased survival of metastatic patients, with successive addition of different treatment modalities [5].

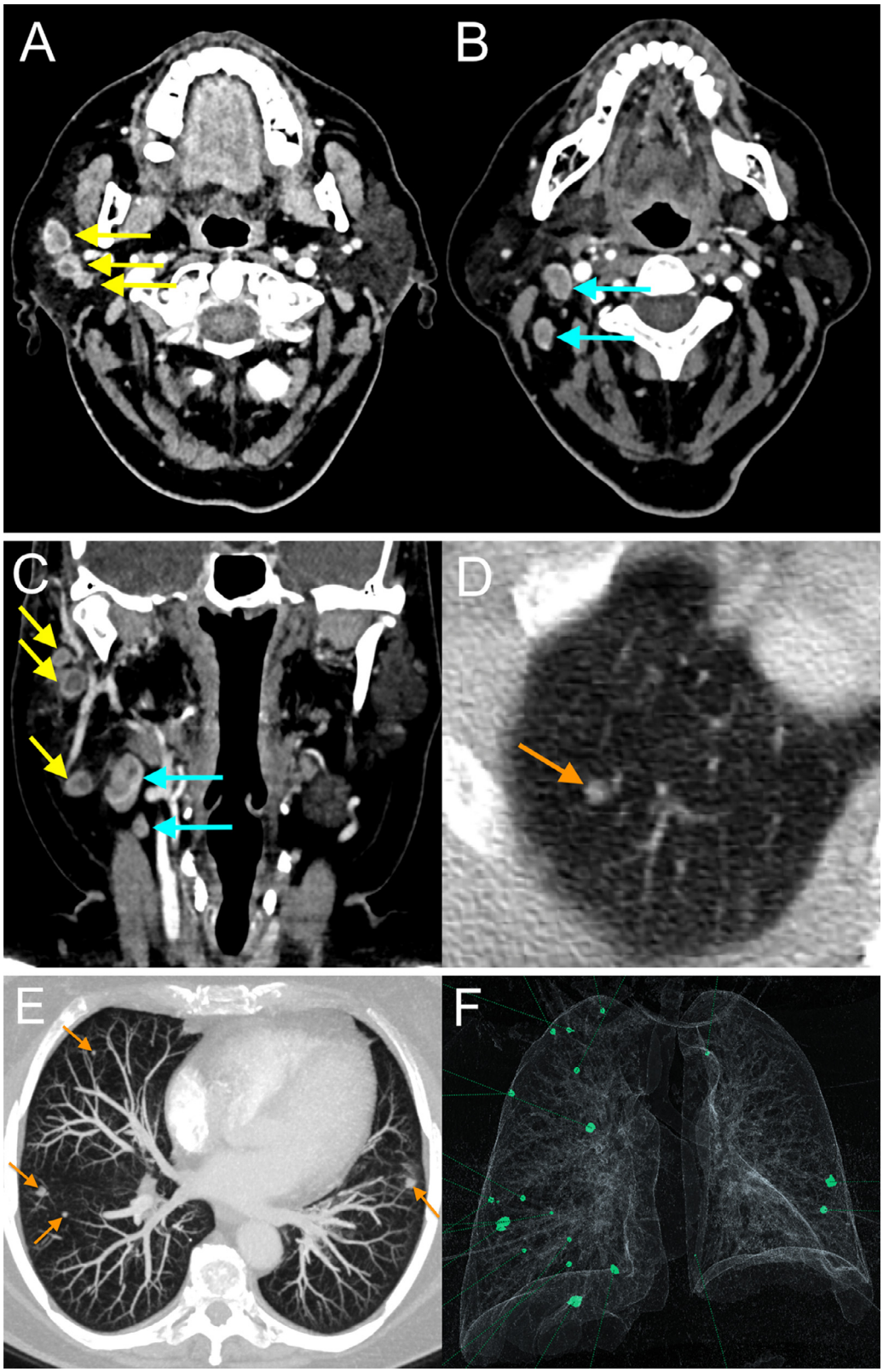

Fig. 7 – Venous phase contrast-enhanced CT of the neck and chest 5.5 months after presentation. (A-C) CT of the neck demonstrating multiple suspect lymph nodes in the right parotid gland (yellow arrows) and right cervical levels 2-3 (blue arrows). (D) Lung window showing one of multiple millimetric solid lung nodules in the right upper lobe (orange arrow). (E) Chest CT maximum intensity projection (MIP) performed 3 days later showing bilateral solid lung nodules, not demonstrated on preoperative imaging (orange arrows). (F) 3D volume rendering reconstruction showing bilateral metastases (green nodules), predominantly in the right lung.

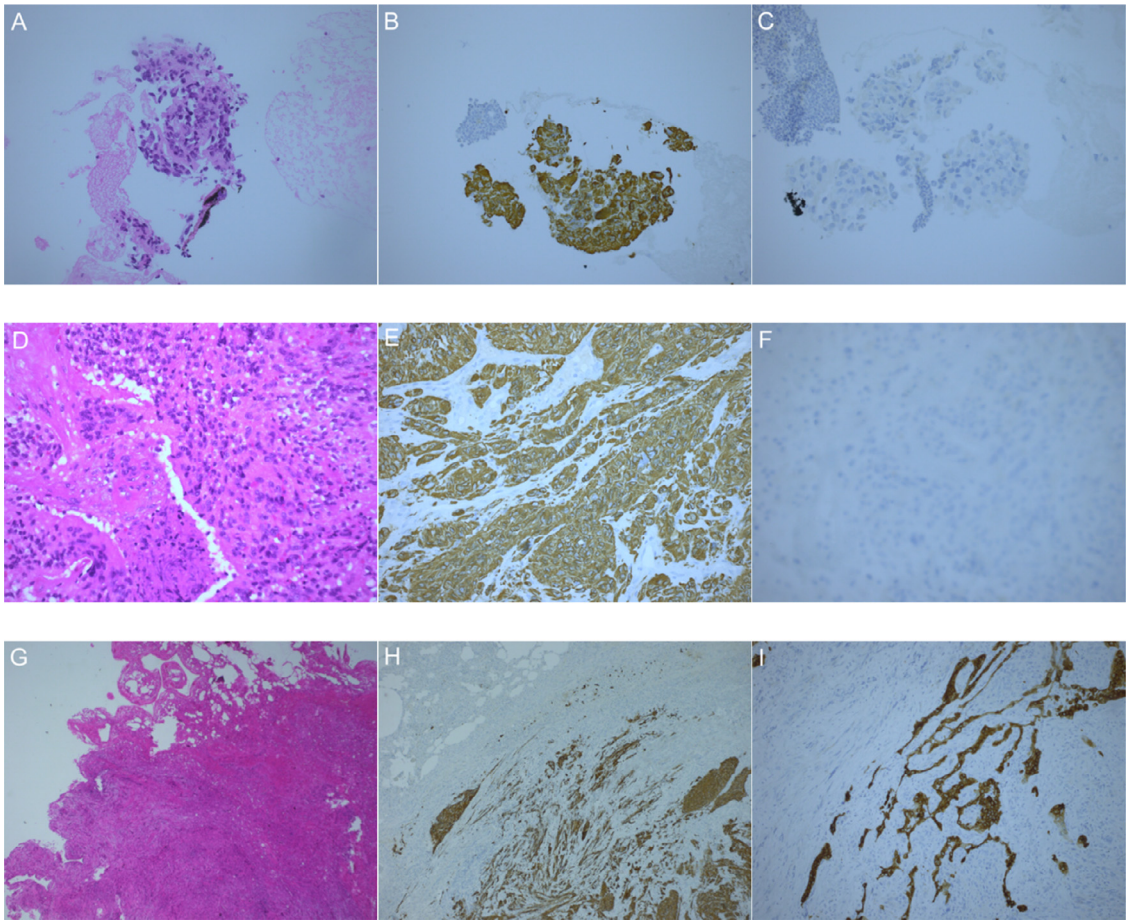

Fig. 8 – Parotid, cervical lymph node and lung nodule tissue morphologic aspects and immunohistochemical staining. (A-C) Fine-needle aspiration cytology of a parotid lesion (20×). (A) H&E stain on tissue block showing atypical cells. (B) Atypical cells express GFAP (brown staining) (C) and are pankeratin negative, unusual for parotid gland neoplasm. (D-F) Biopsy of a cervical lymph node (20×). (D) H&E stain showing similar atypical cells (E) with expression of GFAP and (F) pankeratin negative staining. (G-I) Thoracoscopic biopsy of a lung nodule. (G) H&E (2.5×) stain showing a tumoral nodule. (H) Tumoral cells are GFAP positive (2.5×) and (I) pankeratin negative (pankeratin positive brown cells are entrapped alveoli) (10×).

As our patient developed metastases while receiving radiotherapy and chemotherapy treatment according to Stupp protocol, the patient was referred to an external center for experimental treatment [17]. In a clinical trial setting, the patient received a combination of axitinib (VEGFR 1-3 inhibitor) and avelumab (anti-PD-L1 IgG1 antibody). According to external reports, this treatment regimen might have had a short-term effect, as imaging findings were stable for approximately 1.5 months. Unfortunately, the patient subsequently deteriorated rapidly. Therapy was finally changed to an alkylating agent monotherapy (lomustine) but was unable to stabilize decline. Although many new therapeutic options are currently under study, the effectiveness remains unclear for most agents. As the median age of patients with extraneural GBM metastases is only 38-42 years, an aggressive treatment approach seems justifiable. However, aggressive treatment should always be weighted against best supportive care, depending on the patient's individual wish and context [3].

Conclusions

As the number of long-term GBM survivors will likely increase, the incidence of extracranial metastases is expected to rise. Detection of GBM metastases may therefore become more common and clinically relevant. Routine follow-up scans can show unexpected extraneural metastases. Radiologists should be aware of this possibility to correctly detect and interpret metastatic GBM disease.

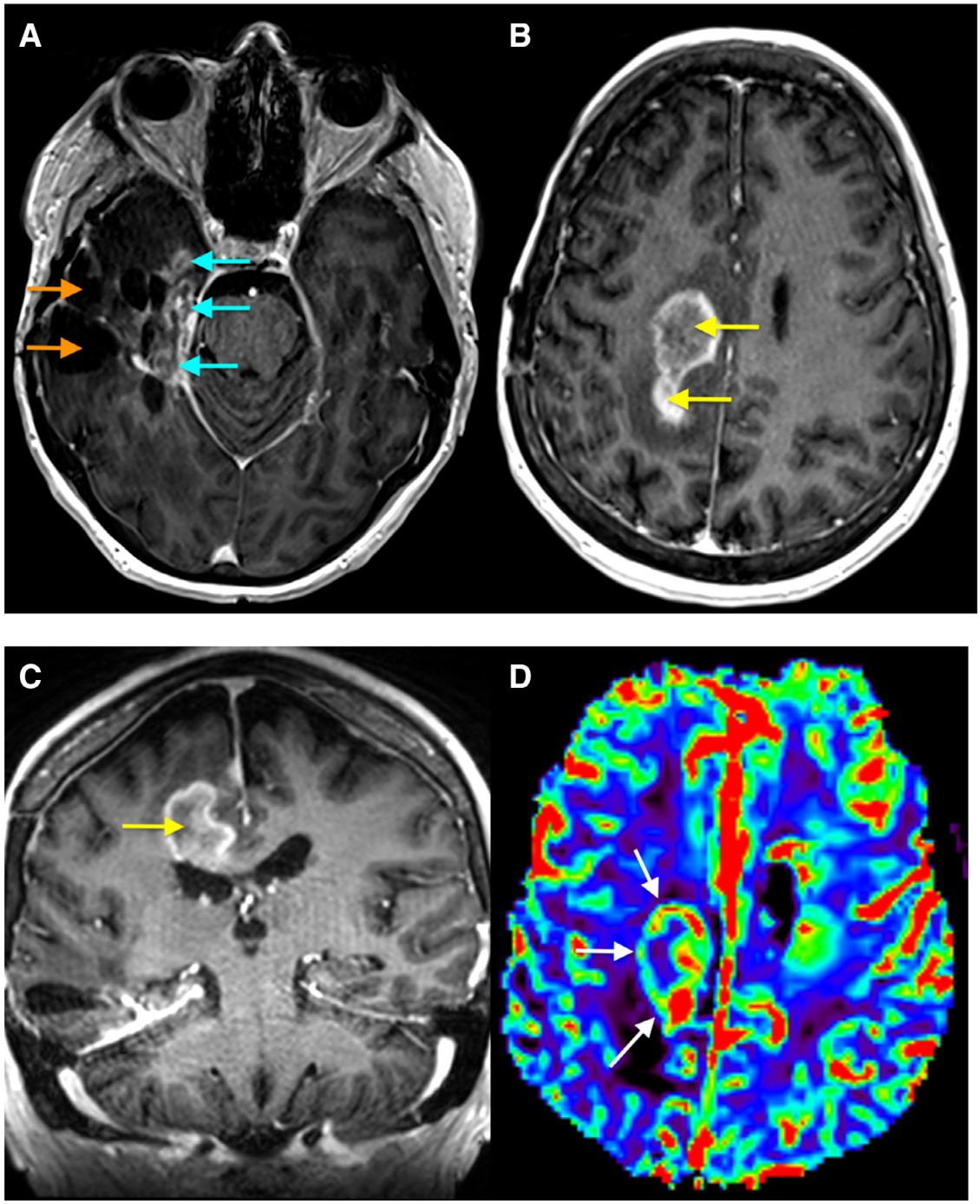

Fig. 9 – MRI of the brain 12.5 months after presentation. (A) Gadolinium-enhanced T1-weighted image showing local recurrence (blue arrow) and cystic encephalomalacia of the resection cavity (orange arrow). (B-C) Additionally, a contrast-enhancing mass (yellow arrows) was present in the right superior frontal gyrus and body of the corpus callosum. (D) Perfusion-weighted image showing an increased rCBF (white arrows) in the area of the frontocallosal mass. (E-F) T2-FLAIR-weighted images showing hyperintensity of the mass (red arrow) with significant perilesional edema (green arrows) extending to the precentral gyrus (purple arrow) and to a lesser extent to the postcentral gyrus (brown arrow), providing a possible explanation for the patient's progressive left-sided hemiparesis.

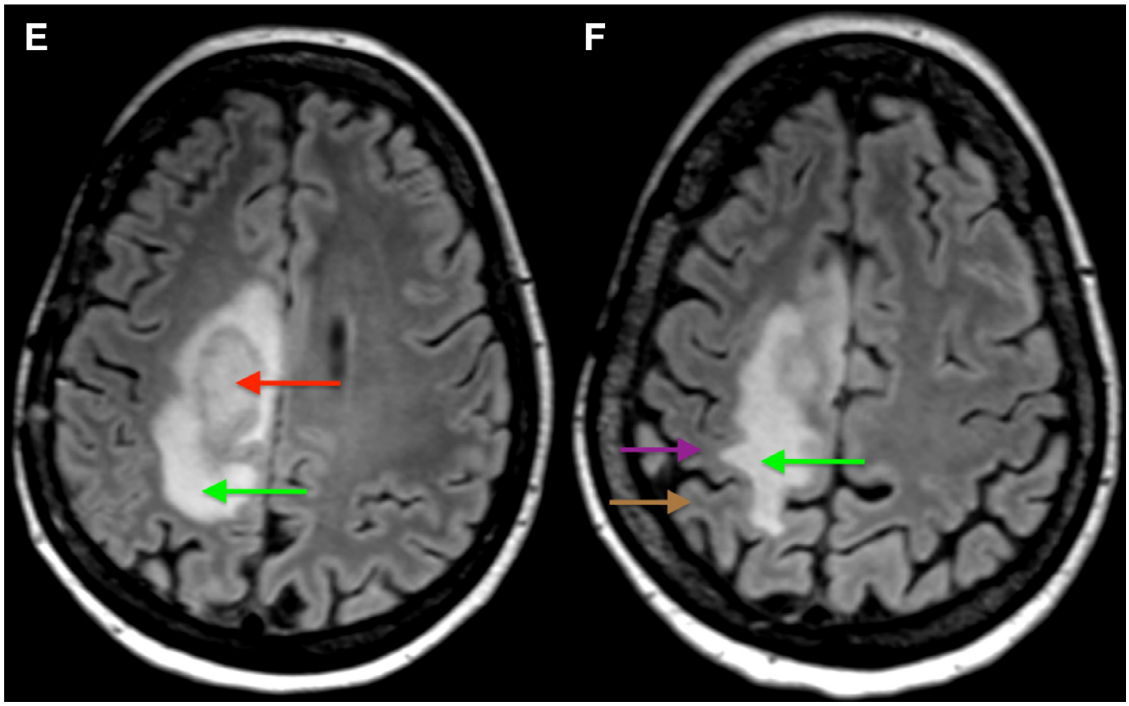

Fig. 9 – Continued

REFERENCES

[1] Ostrom QT, Gittleman H, Truitt G, Boscia A, Kruchko C, Barnholtz-Sloan JS. CBTRUS statistical report: primary brain and other central nervous system tumors diagnosed in the United States in 2011-2015. Neuro Oncol 2018;20(suppl_4): iv1–iv86.

[2] Louis DN, Perry A, Reifenberger G, von Deimling A, Figarella-Branger D, Cavenee WK, et al. The 2016 World Health Organization classification of tumors of the central nervous system: a summary. Acta Neuropathol 2016;131(6):803–20.

[3] Pietschmann S, Von Bueren AO, Kerber MJ, Baumert BG, Kortmann RD, Müller K. An individual patient data meta-analysis on characteristics, treatments and outcomes of glioblastoma/gliosarcoma patients with metastases outside of the central nervous system. Dehghani F. PLoS One 2015;10(4):e0121592.

[4] Piccirilli M, Brunetto GMF, Rocchi G, Giangaspero F, Salvati M. Extra central nervous system metastases from cerebral glioblastoma multiforme in elderly patients. Clinico-pathological remarks on our series of seven cases and critical review of the literature. Tumori 2008;94(1):40–51.

[5] Lun M, Lok E, Gautam S, Wu E, Wong ET. The natural history of extracranial metastasis from glioblastoma multiforme. J Neurooncol 2011;105(2):261–73 .

[6] Blume C, Von Lehe M, Van Landeghem F, Greschus S, Boström J. Extracranial glioblastoma with synchronous metastases in the lung, pulmonary lymph nodes, vertebrae, cervical muscles and epidural space in a young patient—case report and review of literature. BMC Res Notes 2013;6(1):290.

[7] Romero-Rojas AE, Diaz-Perez JA, Amaro D, Lozano-Castillo A, Chinchilla-Olaya SI. Glioblastoma metastasis to parotid gland and neck lymph nodes: fine-needle aspiration cytology with histopathologic correlation. Head Neck Pathol 2013;7(4):409–15.

[8] Taha M, Ahmad A, Wharton S, Jellinek D. Extra-cranial metastasis of glioblastoma multiforme presenting as acute parotitis. Br J Neurosurg 2005;19(4):348–51.

[9] Kuhn U, Kohler HH, Jecker P. Rare tumors of the parotid gland. Lymphadenoma of a sebaceous gland and extracranial metastasis from glioblastoma. HNO 2003;51(5):417–20.

[10] Megele R, Gruß P, Bührmann K. Das extrakraniell metastasierende maligne Gliomiatrogen. Minim Invasive Neurosurg 1989;32(05):157–9.

[11] Moghtader A. Cervical and parotid metastasis secondary to cerebral astrocytoma. Laryngoscope 1966;76(11):1834–41.

[12] Ogungbo BI, Perry RH, Bozzino J, Mahadeva D. Report of GBM metastasis to the parotid gland. J Neurooncol 2005;74(3):337–8.

[13] Waite KJ, Wharton SB, Old SE, Burnet NG. Systemic metastases of glioblastoma multiforme. Clin Oncol (R Coll Radiol) 1999;11(3):205–7.

[14] Taskapilioglu MO, Aktas U, Eser P, Tolunay S, Bekar A. Multiple extracranial metastases from secondary glioblastoma: a case report and review of the literature. Turk Neurosurg 2013;23(6):824–7.

[15] Kraft M, Lang F, Braunschweig R, Janzer RC. Parotid gland metastasis from glioblastoma multiforme: a case report and review of the literature. Eur Arch Otorhinolaryngol 2008;265(6):709–11.
[16] Park CC, Hartmann C, Folkerth R, Loeffler JS, Wen PY, Fine HA, et al. Systemic metastasis in glioblastoma may represent the emergence of neoplastic subclones. J Neuropathol Exp Neurol 2000;59(12):1044–50.
[17] Stupp R, Mason WP, van den Bent MJ, Weller M, Fisher B, Taphoorn MJ, et al. Radiotherapy plus concomitant and adjuvant temozolomide for glioblastoma. N Engl J Med 2005;352(10):987–96.
[18] Seifert G, Hennings K, Caselitz J. Metastatic tumors to the parotid and submandibular glands: analysis and differential diagnosis of 108 cases. Pathol Res Pract 1986;181(6):684–92.
[19] Alphandéry E. Glioblastoma treatments: an account of recent industrial developments. Front Pharmacol 2018;9:879.
[20] Müller C, Holtschmidt J, Auer M, Heitzer E, Lamszus K, Schulte A, et al. Cancer: hematogenous dissemination of glioblastoma multiforme. Sci Transl Med 2014;6(247) 247ra101.